

This is a repository copy of *Competition between mass-symmetric and asymmetric fission modes in 258Md produced in the 4He+254Es reaction*.

White Rose Research Online URL for this paper:

<https://eprints.whiterose.ac.uk/225665/>

Version: Accepted Version

Article:

Nishio, K., Hirose, K., Makii, H. et al. (33 more authors) (2025) Competition between mass-symmetric and asymmetric fission modes in 258Md produced in the 4He+254Es reaction. *Physical Review C*. 044609. ISSN 2469-9993

<https://doi.org/10.1103/PhysRevC.111.044609>

Reuse

This article is distributed under the terms of the Creative Commons Attribution (CC BY) licence. This licence allows you to distribute, remix, tweak, and build upon the work, even commercially, as long as you credit the authors for the original work. More information and the full terms of the licence here:

<https://creativecommons.org/licenses/>

Takedown

If you consider content in White Rose Research Online to be in breach of UK law, please notify us by emailing eprints@whiterose.ac.uk including the URL of the record and the reason for the withdrawal request.

Competition between mass-symmetric and asymmetric fission modes in ^{258}Md produced in the $^4\text{He} + ^{254}\text{Es}$ reaction

K. Nishio^{1,*}, K. Hirose¹, H. Makii¹, R. Orlandi¹, K.R. Kean^{2,1}, K. Tsukada^{1,†}, A. Toyoshima¹, M. Asai¹, T.K. Sato¹, N.M. Chiera¹, T. Tomitsuka^{3,1}, K. Tokoi^{4,1}, R. Yanagihara^{5,1}, H. Suzuki^{4,1}, Y. Nagame¹, K. Okada¹, A.N. Andreyev^{6,1}, T. Tanaka^{7,8}, K. Morimoto⁷, S. Ishizaki⁹, M. Okubayashi⁹, Y. Miyamoto⁹, S. Tanaka⁹, S. Takagi⁹, Y. Aritomo⁹, S. Kubono⁷, N. Iwasa¹⁰, M. Egeta¹⁰, S. Sakaguchi⁸, S. Matsunaga⁸, Y. Ishibashi⁸, K.P. Rykaczewski¹¹, R.A. Boll¹¹, J.G. Ezold¹¹, L.K. Felker¹¹, and J.B. Roberto¹¹

¹ *Advanced Science Research Center, Japan Atomic Energy Agency, Tokai, Ibaraki 319-1195, Japan*

² *Laboratory for Advanced Nuclear Energy, Institute for Innovative Research, Tokyo Institute of Technology, Tokyo 152-8550, Japan*

³ *Graduate School of Science and Technology, Niigata University, Niigata 950-2181, Japan*

⁴ *Graduate School of Science and Engineering, Ibaraki University, Ibaraki 310-8512, Japan*

⁵ *Research Center for Nuclear Physics, Osaka University, Osaka 567-0047, Japan*

⁶ *School of Physics, Engineering and Technology, University of York, York YO10 5DD, United Kingdom*

⁷ *RIKEN Nishina Center for Accelerator-Based Science, Saitama 351-0198, Japan*

⁸ *Department of Physics, Kyushu University, Fukuoka 819-0395, Japan*

⁹ *Faculty of Science and Engineering, Kindai University, Higashi-Osaka, Osaka 577-8502, Japan*

¹⁰ *Department of Physics, Tohoku University, Sendai 980-8578, Japan and*

¹¹ *Oak Ridge National Laboratory, Oak Ridge, Tennessee 37831, USA*

(Dated: April 13, 2025)

Earlier studies of spontaneous fission of heavy actinides found that the fission fragments mass distribution suddenly changes from predominantly asymmetric to symmetric, when the mass number of the fissioning nucleus becomes larger than $A_c=257$. We have measured for the first time fission-fragment mass and total-kinetic-energy (TKE) distributions of the excited compound nucleus $^{258}\text{Md}^*$ ($Z=101$), populated in the reaction $^4\text{He}+^{254}\text{Es}$, using the rare radioactive target isotope ^{254}Es with a short half-life, $T_{1/2}=275.7$ d. The fission of $^{258}\text{Md}^*$ can be interpreted as involving 3 fission modes: one mass-asymmetric and two mass-symmetric fission modes, the latter two are manifested by different TKE values. In this assumption, symmetric and asymmetric fission modes have nearly similar yields at the excitation energy of 15.0 MeV. The spectrum of 18.0 MeV can be explained as due to the increase of asymmetric fission mode.

I. INTRODUCTION

Shortly after the discovery of nuclear fission in 1938 [1, 2], the fundamental concept to describe fission was established by analogy with the behavior of a charged liquid drop. Fission happens in a heavy nucleus when the repulsive Coulomb energy between the constituent protons overwhelms the attractive surface energy [3]. Such a classical treatment, however, cannot explain the mass asymmetric fission producing two unequal fragments of actinide nuclei, which was known already at the dawn of fission research. To describe asymmetric fission, nuclear shell effects have to be introduced [4–7]. By adding extra binding energy originating from the shell structure [8, 9], the classically predicted smooth potential energy surface (PES) of a liquid-drop nucleus with a single symmetric fission valley is largely changed to a more complex PES with possibly, a number of different fission paths (modes), see Fig.1 of [10]. The modes can be distinguished both by their fission-fragment mass distributions (FFMDs) and respective total kinetic energies (TKEs), resulting from

different scission configurations [11]. It is important to note that both PES and resulting FFMDs strongly depend on the excitation energy, often leading to the transition from asymmetric FFMD at low excitation-energy to broader symmetric distribution toward high energies [12], due to washing out of the shell effects.

In spontaneous fission (SF) the mass-asymmetric FFMDs for actinides are known to dramatically change to symmetric fission when the mass of fissioning nucleus exceeds $A_c=257$, see Fig. 1. Below $A_c=257$, the FFMD and TKE distributions are frequently interpreted as involving three fission modes [11], i.e., two mass-asymmetric, called Standard 1 (ST1) and Standard 2 (ST2), and one symmetric fission modes, Superlong (SL). The typically weak ST1 is characterized by a heavy-fragment nuclear charge of $Z_H \approx 52$, while the dominant ST2 mode is stabilization at $Z_H=54-56$ over the wide range of fissioning nuclei [14–17]. The origin of ST2 was recently interpreted as due to the onset of octupole (pear-shaped) deformation of the nascent heavy fragment [18]. The SL is characterized by low TKE values, typically $\approx 150-160$ MeV [11], indicating strongly-deformed fragments (thus the larger distance between their centers). In SF of $A_c > 257$ shown in Fig. 1, the so-called Supershort (SS) mode [11] is found in $^{258,259}\text{Fm}$, $^{259,260}\text{Md}$ and ^{262}No [19–23], which

* nishio.katsuhisa@jaea.go.jp

† kazu.tsukada@raris.tohoku.ac.jp

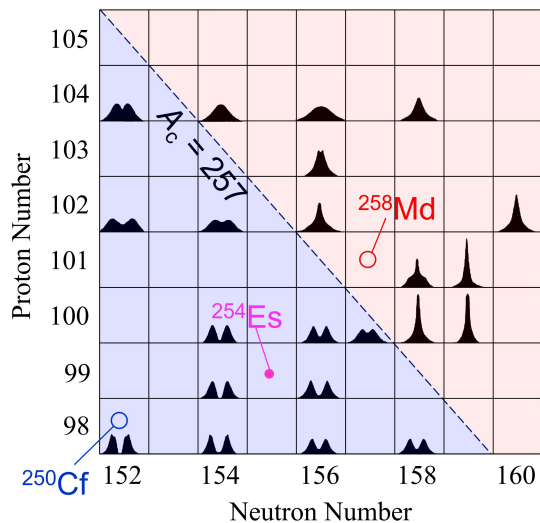


FIG. 1. (Color online) Fission fragment mass distributions in spontaneous fissions. The figure is based on [13]. The target nucleus ^{254}Es and the nuclides studied in the present experiment ($^{258}\text{Md}^*$ and ^{250}Cf) are indicated. The regions with $A_c < 257$ and $A_c > 257$, characterized by mass-asymmetric and mass-symmetric FFMD, respectively, are shown in different colors.

has large TKE of ≈ 233 MeV, due to the production of two identical fragments close to the doubly-magic ^{132}Sn . Furthermore there is other symmetric fission path characterized by its TKE of ≈ 200 MeV, evidently lower than the SS mode but higher than the SL mode. We call it the Short (SH) mode in the discussion hereafter. While the nuclides with $A_c > 257$ can be interpreted as having co-existence of the symmetric SS and SH modes (or only SH mode for $^{258,260}\text{Rf}$ [20, 22]), no clear signature and detailed properties for SL and asymmetric fission modes have been argued in this region.

Furthermore, in the fission of $A_c > 257$, little is investigated about the fission from low excited states. By changing the excitation energy of ^{258}Fm from 0 MeV in SF to 6.23 MeV in neutron-capture of ^{257}Fm , the FFMD changes to a broad symmetric shape by losing its pronounced peak structure [24, 25]. The change of the FFMD is very significant in contrast to fission in the region of $A_c < 257$, where the change of FFMDs between SF and neutron-induced fission is very small [12]. More high-energy fission data in this region are available in $^{257}\text{Md}^*$ ($E^* > 37.5$ MeV) [26] and $^{260}\text{No}^*$ ($E^* = 41$ MeV) [27]. But, in such an energy, shell effects would be weakened.

In this article, we report on the fission study of $^{258}\text{Md}^*$, the nucleus located just above the $A_c = 257$ line, produced in the $^4\text{He} + ^{254}\text{Es}$ reaction. Although fission measurement was attempted in this reaction in the past [28], no data on the FFMD and TKE distributions were reported. Our measurements were done at excitation energies of $E^* = 15.0$ and 18.0 MeV, where shell effects in fission are

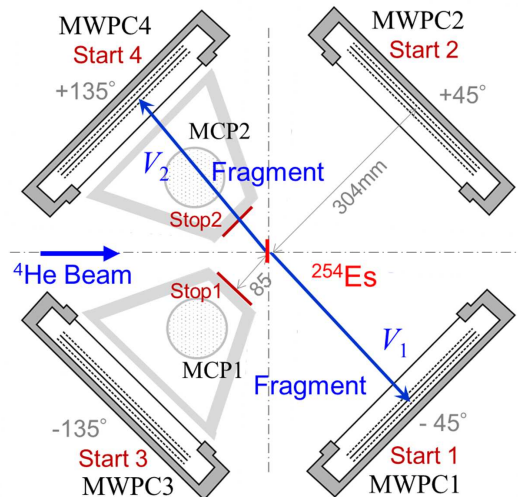


FIG. 2. (Color online) Experimental setup for ^4He -induced fission of ^{254}Es .

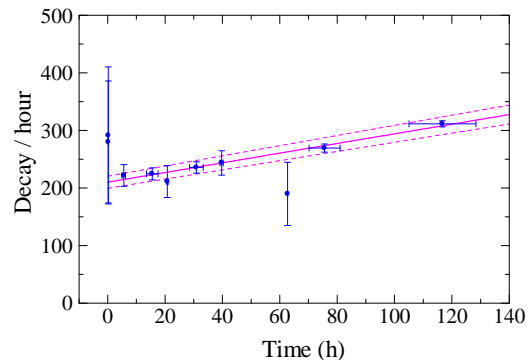


FIG. 3. (Color online) Counting rate of spontaneous fission of ^{250}Cf , measured during the 'beam-off' intervals. Solid line is the calculated accumulation of $^{250}\text{Cf}(\text{SF})$ using decay properties starting from ^{254}Es . Dashed curve is the 5% error.

expected to survive [29]. We observed the change of fragment mass and TKE distribution between two excitation energies. The data are interpreted assuming three fission modes; Asymmetric (AS), Short (SH) and Super-long (SL). Use of the very rare material ^{254}Es with short half-life ($T_{1/2} = 275.7$ d) [30], currently produced only at the High Flux Isotope Reactor (HFIR) [31] and chemically separated at the adjacent Radio-Engineering Development Center (REDC) of Oak Ridge National Laboratory (US), made this experiment possible.

II. EXPERIMENT

A. Experimental setup

We used a ^4He beam extracted from the ECR ion source installed on the high-voltage terminal of the JAEA

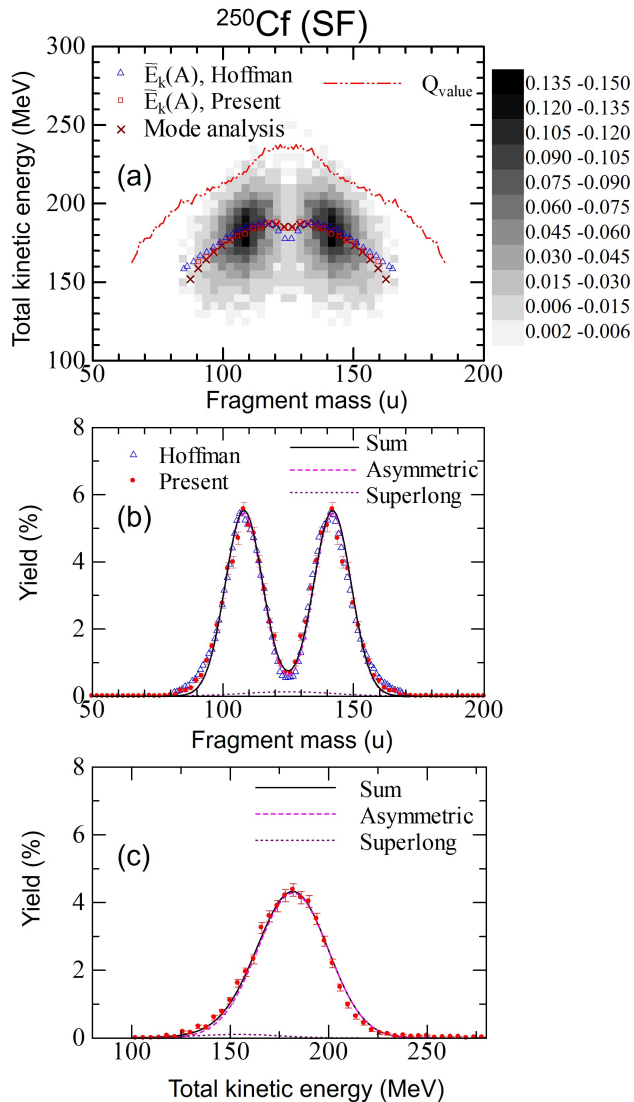


FIG. 4. (Color online) (a) Fission-fragment yield on the mass-TKE ($A-E_k$) plane for $^{250}\text{Cf}(\text{SF})$. The scale is normalized such that the total yield gives 200%. The darkest cell corresponds to the highest yield in the obtained spectrum. The lightest plot is given when more than two events appears in each cell $(\Delta A, \Delta E_k) = (3 \text{ u}, 5 \text{ MeV})$. The average TKE for each mass $\bar{E}_k(A)$ (solid rectangle) is shown. The data are compared with those from Hoffman *et al.* [33]. The $\bar{E}_k(A)$ from the mode analysis is shown by cross symbol, see the discussion in Sec. III. The dash-dot-dot curve is the fission Q-values. (b)(c) Projection of the events on A and E_k (solid circles). The FFMD and TKE distributions for each fission mode obtained in the analysis (asymmetric and superlong) are shown as well as their sum, see Sec. III.

tandem accelerator. The experimental setup is shown in Fig. 2. Two beam energies of 22.6 and 25.7 MeV, corresponding to $E^* = 15.0$ and 18.0 MeV, respectively, were used. The typical beam current was ≈ 9 pA.

Masses and total kinetic energies of both fragments in the fission of $^{258}\text{Md}^*$ were determined by the so-

called double-velocity method, where two fragment velocities (V_1 and V_2) were independently obtained by a time-of-flight technique. As the average fragment velocity $\bar{V}_{1,2}$ does not change after prompt-neutron emission from the fragment, the method gives pre-neutron emission fragment mass and TKE. The setup consists of two sets of double-TOF array mounted in the directions of $(+45^\circ, -135^\circ)$ and $(-45^\circ, +135^\circ)$, respectively. The fission fragments are detected in coincidence by a pair of multi-wire proportional counters (MWPC1 & MWPC4 and MWPC2 & MWPC3), used for the stop signal. The start timing signal was obtained by detecting electrons ejected when a fragment passes a thin foil ($0.5 \mu\text{m}$ Mylar film coated by $30 \mu\text{g}/\text{cm}^2$ gold layer), where electrons were guided by the electrostatic mirror to the microchannel plate (MCP) detector to multiply electrons. The mass and TKE resolution of the detector setup is $\sigma_A = 2.9 \text{ u}$ and $\sigma_{\text{TKE}} = 3.6 \text{ MeV}$, obtained in the elastic scattering in the $^{36}\text{Ar} + ^{142}\text{Nd}$ reaction [32].

B. ^{254}Es Target fabrication

The target was prepared by electrodeposition of the 10-ng ^{254}Es material (0.69 MBq) with a 2.0-mm diameter ($0.32 \mu\text{g}/\text{cm}^2$) on a $270 \mu\text{g}/\text{cm}^2$ nickel foil. The deposition-layer side was covered by the nickel foil with the same thickness to prevent the deposited material recoiled out of the target layer by α -decay. Before the electrodeposition, we made a chemical separation to extract einsteinium that contains other actinides and lanthanides. The fraction of ^{253}Es ($T_{1/2} = 20.47 \text{ d}$) [30], the only einsteinium contamination, was determined to be $^{253}\text{Es}/^{254}\text{Es} = 2.0 \times 10^{-5}$ at the time of the experimental run, as it had almost decayed out after the production in the HFIR. During the experiment the nucleus ^{250}Cf (13.08 y) is produced as a granddaughter via $^{254}\text{Es}(\alpha: 100.00\%) \rightarrow ^{250}\text{Bk}(3.21 \text{ h}, \beta^-: 100\%) \rightarrow ^{250}\text{Cf}(\alpha: 99.92\%, \text{SF}: 0.08\%)$ [30]. The SF of ^{250}Cf was recorded intermittently by stopping the beam, for the calibration of the measuring system by referring to the literature data [33].

The ^{250}Cf is accumulated in the target material nearly linearly with time. Monitoring of the spontaneous fission (SF) counting rate with the 'beam-off' condition allows to check the stability and the content of the ^{254}Es target material. In particular, the SF rate of ^{250}Cf is important as it has to be subtracted as background (BG) from the spectra of the ^4He -beam run to obtain pure fission data of ^{258}Md .

The SF activity from ^{250}Cf is shown in Fig. 3 as a function of time during and after the beam measurement. This was obtained by the number of coincidence events of both fragments. Solid line is the calculated accumulation of $^{250}\text{Cf}(\text{SF})$ with time, starting from the purification date of 20th June, 2018. The $Time=0$ of this figure is the first measurement of $^{250}\text{Cf}(\text{SF})$ activity (1st July 2018). The line can well describe the trend of accumul-

ing ^{250}Cf by assuming that the initial ^{254}Es material is 10.5 ng at 20th June and ^{250}Cf was fully removed in the process of extracting the einsteinium. The data points follow the curve within the uncertainty level of $\pm 5\%$, shown by the dashed lines on both sides of the solid line. The solid curve is used to estimate the amount of contaminated BG of $^{250}\text{Cf}(\text{SF})$ during the beam run. Uncertainly in the fission-fragment mass and total kinetic energy distributions originating from the 5% systematic error in background subtraction is smaller than the statistical error, shown in Fig. 7 and Fig. 8.

We also checked the amount of the ^{254}Es material in the target before and after the experiment by measuring the γ -rays following the β^- decay of ^{250}Bk . After accounting for the reduction of the ^{254}Es material due to the decay, the amount before and after the measurement agreed within 6%, comparable with the uncertainty from the statistical error and γ -ray detection-efficiency.

C. Experimental data

1. $^{250}\text{Cf}(\text{SF})$

To benchmark the target, detection system and analysis procedure, we show the results for $^{250}\text{Cf}(\text{SF})$ in Fig. 4. The panel (a) provides the mass-TKE distribution. Projection of the events on the fragment mass and TKE axis are shown in (b) and (c), respectively (solid circles). We note that 2D plots have a larger bin-size for the mass and TKE to give a proper statistics for each cell. The FFMD has a Gaussian-like heavy- and light-fragment distributions at the average heavy-fragment mass $\bar{A}_H=142.2\pm 0.5$, in good agreement with the data of [33]. The average charge of heavy-fragments $Z_H=55.6$, estimated from the assumption of unchanged-charge-density (UCD), locates within $Z_H=52-56$. The average TKE, $\bar{E}_k = 180.2\pm 1.0$ MeV, agrees with 184.3 ± 2.7 MeV in [33], which was obtained by measuring kinetic energies of both fragments. Dependence of the average TKE for each fragment mass, $\bar{E}_k(A)$, is shown in Fig. 4(a). The curve follows a quadratic shape, but has a local minimum at the symmetric fission. The minimum indicates the presence of the SL mode, which is discussed below. This benchmark of $^{250}\text{Cf}(\text{SF})$, which gives good agreement between literature results and our data, establishes confidence in our analysis of $^{258}\text{Md}^*$.

2. Folding angle distribution of fission fragments

In the $^4\text{He}+^{254}\text{Es}$ run which gives $E^*=18.0$ -MeV for $^{258}\text{Md}^*$, about 17,500 fission-coincidence events were accumulated, including a $9.1\pm 0.5\%$ contribution from SF(^{250}Cf), which was further subtracted in the analysis. For the $E^*=15.0$ -MeV, about 10,900 events were accumulated, containing $40.7\pm 2.0\%$ from $^{250}\text{Cf}(\text{SF})$. The data analysis process is as follows. First, by using the data

files of the beam-on run, which include fission events from $^{258}\text{Md}^*$ and $^{250}\text{Cf}(\text{SF})$, we adopted the fissioning nucleus mass $A_c=258$ and its recoil energy in the $^4\text{He}+^{254}\text{Es}$ reaction. The ^{250}Cf spectrum to be subtracted is created with the same assumption, but using the files of beam-off period. We measured that the fission rate of $^{258}\text{Md}^*$ at the 18.0 MeV-run normalized to the beam dose is 6.8 times larger than the fission rate of the 15.0 MeV-run. We also note that fission events associated with $^4\text{He}+^{250}\text{Cf}$ are only 1.6% of those from $^4\text{He}+^{254}\text{Es}$ on average during the run, thus no correction for this effect was performed.

In order to demonstrate the correctness of subtracting background fissions originating from $^{250}\text{Cf}(\text{SF})$, we show the folding-angle distribution between two fission fragments in the laboratory frame (θ and ϕ), as defined in Fig. 5. Fig. 5 (a1) and (a2) show the folding angle spectra for $E_{\text{beam}}=22.6$ MeV ($E^*=15.0$ MeV). Open red circles are the spectra obtained during the beam irradiation, in which $^{250}\text{Cf}(\text{SF})$ BG is included. The estimated BG component is shown by open black circles. The solid red circles are the net spectrum for fission of ^{258}Md , obtained after subtracting the BG. Similarly, we obtained the spectra for $E_{\text{beam}}=25.7$ MeV ($E^*=18.0$ MeV) in the panels of (b1) and (b2). In Fig. 5(c1) and (c2), we show the normalized folding-angle distributions for $^{258}\text{Md}^*$, which are compared to $^{250}\text{Cf}(\text{SF})$. The θ distribution for $^{258}\text{Md}^*$ has a peak around $\theta=177^\circ$ due to recoil of the fissioning nucleus, in contrast to $^{250}\text{Cf}(\text{SF})$ centered at 180° . The 18.0-MeV distribution locates at slightly smaller angle than 15.0-MeV data, due to larger recoil energy. The normalized spectra of ϕ in (c2) for both $^{258}\text{Md}^*$ data almost agree with each other. This indicates the validity of BG correction for $^{258}\text{Md}^*$ data.

3. Results for ^{258}Md fission

The 2D plots on the mass and TKE of fragments from fission of $^{258}\text{Md}^*$ are shown in Fig. 6. Compared to $^{250}\text{Cf}(\text{SF})$, the 2D spectrum reveals that fission of $^{258}\text{Md}^*$ has larger yield in symmetric fission with TKE widely distributed to the vicinity of fission Q-values. The symmetric component of $E^*=15.0$ MeV data has the largest yield around $E_k=210-220$ MeV. The TKE value is not so large as the Supershort mode having a dominant yield closer to the Q-value. Thus we interpreted the symmetric fission as the Short mode. Furthermore, the asymmetric fission mode is evident, centered at $(A_H, E_k) \approx (145 \text{ u}, 200 \text{ MeV})$. On the other hand, the $E^*=18$ MeV spectrum shows relative enhancement of asymmetric fission yield at the same mass-asymmetry but with lower TKE position, $\approx (145 \text{ u}, 190 \text{ MeV})$. Increase of mass asymmetric fission is noticed in the FFMD shown in Fig. 7 that the $E^*=18.0$ MeV spectrum exhibits a trapezoid shape, contrasted to a Gaussian-like shape of the $E^*=15.0$ MeV spectrum. Projection of the events to the TKE are shown in Fig. 8. We found a change of average TKE-value from $\bar{E}_k = 198.7\pm 1.8$ MeV ($E^*=18.0$ MeV) to 190.0 ± 1.0 MeV

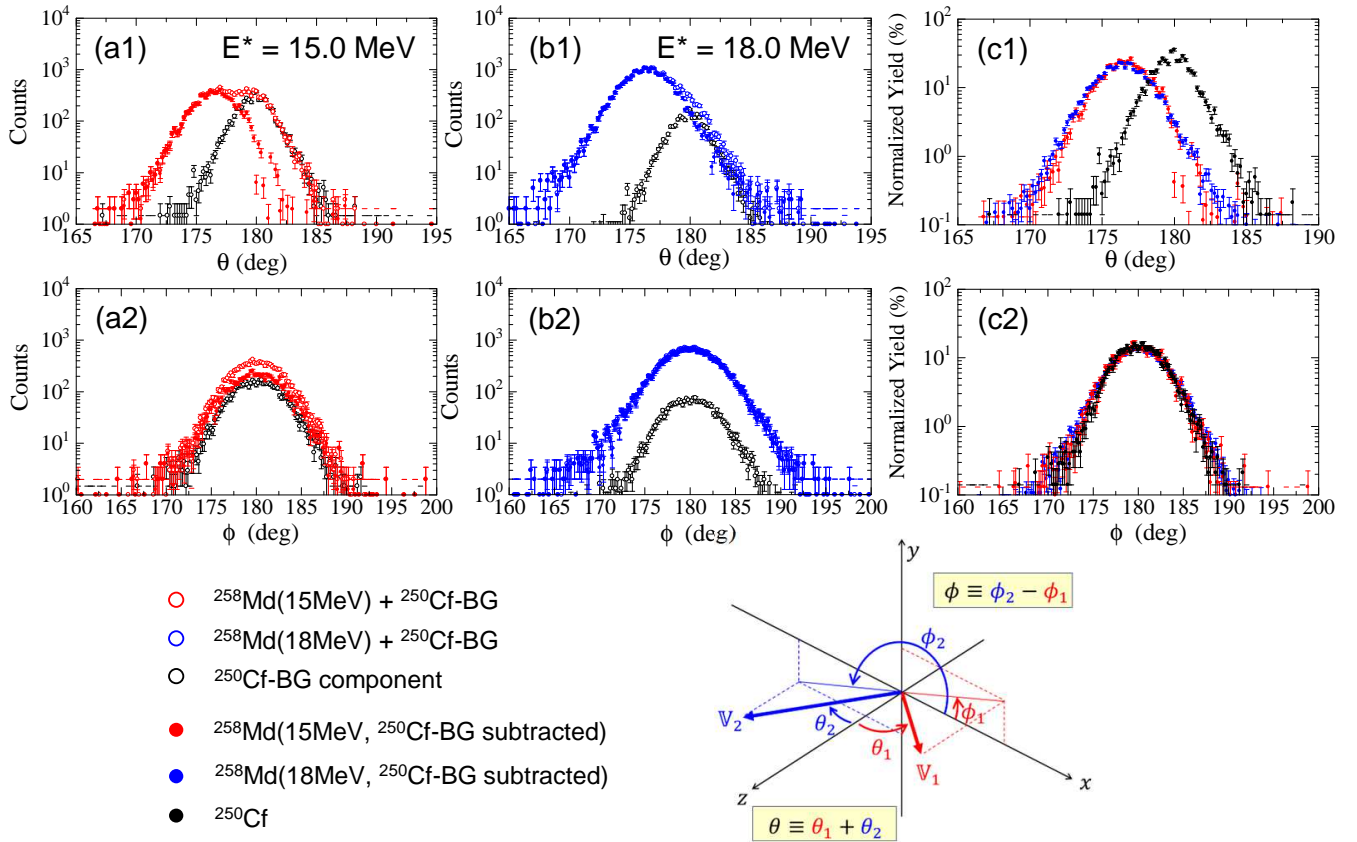


FIG. 5. (Color online) (Bottom left) Folding angle distribution ($\theta = \theta_1 + \theta_2$ and $\phi = \phi_2 - \phi_1$) formed by the flight directions of two fission fragments. (a1)(a2) and (b1)(b2) are the fission spectra for $E^* = 15.0$ and 18.0 MeV run, respectively. Colored open circles are 'beam-on' data, in which BG from ^{250}Cf (SF) is included as shown by black open circle. The net ^{258}Md spectra after subtracting the BG are shown by the colored solid circles. Spectra (c1)(c2) are the normalized yield distribution on θ and ϕ for ^{258}Md (15.0 MeV: red), ^{258}Md (18.0 MeV: blue), and ^{250}Cf (SF) (black).

TABLE I. Fraction of each fission mode for ^{250}Cf (SF) and ^{258}Md ($E^* = 15.0, 18.0$ MeV). Average heavy-fragment mass ($\bar{A}_{H,i}$) and average total kinetic energy ($\bar{E}_{k,i}$) in each fission mode obtained in the analysis are shown inside the parenthesis.

Nucleus (E^*)	Mass Asymmetric		Mass Symmetric	
	Asymmetric (AS)		Short (SH)	Superlong (SL)
^{250}Cf (SF) (0 MeV)	97.0 \pm 2.0% (142.0 u, 181.5 MeV)		-	3.0 \pm 2.0% (125.0 u, 153.1 MeV)
$^{258}\text{Md}^*$ (15 MeV)	52.0 \pm 3.5% (147.0 u, 195.1 MeV)		45.0 \pm 3.5% (129.0 u, 210.0 MeV)	3.0 \pm 1.0% (129.0 u, 148.8 MeV)
$^{258}\text{Md}^*$ (18 MeV)	69.0 \pm 1.0% (144.5 u, 186.4 MeV)		26.0 \pm 1.0% (129.0 u, 210.0 MeV)	5.0 \pm 1.0% (129.0 u, 145.8 MeV)

($E^* = 15.0$ MeV). The former TKE values agree with the Viola formula which gives 197.8 MeV for ^{258}Md [34], but the latter value is ≈ 8 MeV smaller. The rapid change of TKE in such a small excitation-energy change of 3 MeV largely differs from actinide fissions of $A_c < 257$, which show very small change with excitation energy. For example, TKE decreases only 1.3 MeV by gaining 3.0-MeV excitation energy for fission of ^{240}Pu [35]. In the fission-mode analysis shown below in III. DISCUSSION the spectra can be interpreted as the enhancement of the mass asymmetric fission mode at $E^* = 18.0$ MeV.

Change of the intensities for the symmetric and asymmetric fissions are identified by drawing FFMDs using events above and below the arbitrarily chosen E_k value of 200 MeV, see Fig.7. In the $E^* = 15.0$ -MeV spectrum, the high-TKE events have a Gaussian shape, while the low-TKE spectrum exhibits a nearly flat-top trapezoid distribution. By increasing the energy to 18.0 MeV, the low-TKE spectrum create the asymmetric peaks at $A_L/A_H \approx 113/145$ by gaining the yield.

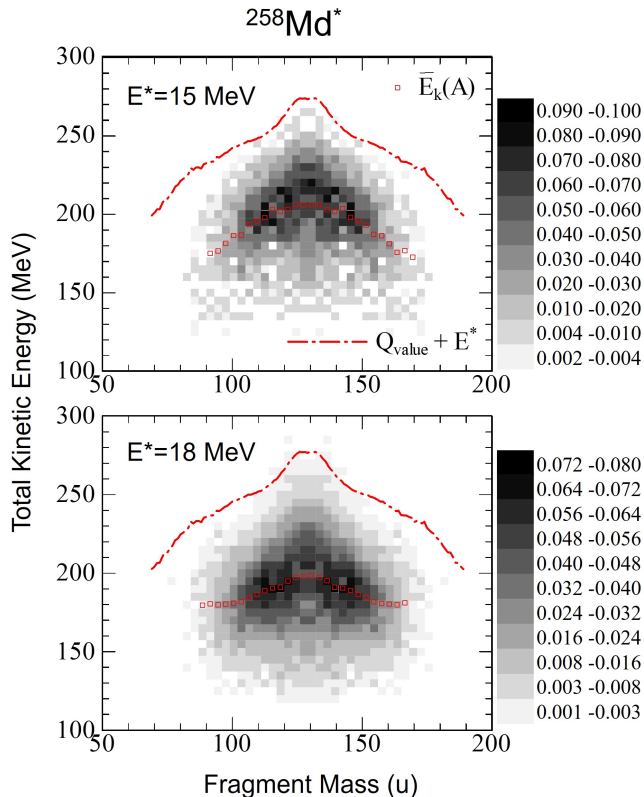


FIG. 6. (Color online) Fission-fragment yield on the mass-TKE ($A-E_k$) plane for $^{258}\text{Md}^*$ for $E^*=15.0$ MeV (upper panel) and 18.0 MeV (lower panel). The scale is normalized such that the total yield gives 200%. The darkest cell corresponds to the highest yield in each spectrum obtained. The lightest plot is given when more than two events appears in each cell ($\Delta A, \Delta E_k$)=(3 u, 5 MeV). The spectra are obtained after subtracting the $^{250}\text{Cf}(\text{SF})$ background. The average TKE for each mass $\bar{E}_k(A)$ (open rectangle) is shown. The dash-dot-dot curves are the sum of the fission Q -values and excitation energy of the compound nucleus.

4. Fission from other reaction

In this section we will discuss the possible influence of fission contaminant from other reactions, particularly multichance fission and the fission of nuclei produced in transfer reactions.

We calculated the probability of 2nd chance fission; i.e., fission of $^{257}\text{Md}^*$ after the neutron emission from CN $^{258}\text{Md}^*$, using the GEF-code [36]. The 2016-version gives a small and similar probability of 5% and 6% at $E^*=15.0$ MeV and 18.0 MeV, respectively. Here, the spins of the CN produced in $^4\text{He}+^{254}\text{Es}$ are taken into account using the code [37]. Thus the difference of the fission properties between $E^*=18.0$ MeV and 15.0 MeV cannot be explained by the $^{257}\text{Md}^*$ contamination. We note that multichance fission probabilities from GEF-2016 version can well explain experimental data of the FFMDs for high-energy fissions of various actinide nu-

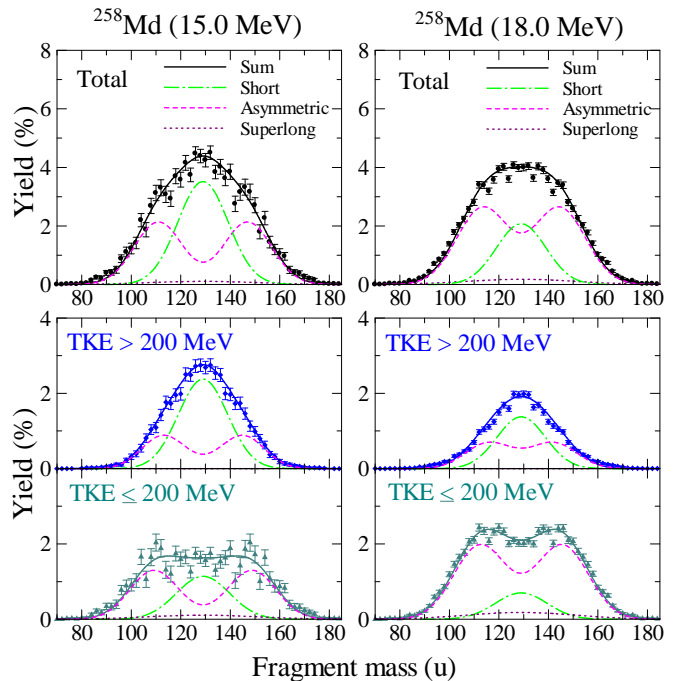


FIG. 7. (Color online) Fission-fragment mass distributions for $^{258}\text{Md}^*$ at excitation energy $E^*=15.0$ MeV (left panels) and 18.0 MeV (right panels). Top figures are FFMDs from all events. Middle and lower panels are the distributions from events above and below the total kinetic energy of $E_k=200$ MeV. Lines are the distributions from each fission mode and their sum. Numerical expressions of the curves are shown in APPENDIX.

clides when they are adopted in the Langevin calculation [29, 38].

The possible contribution from transfer induced fission can be evaluated from the ϕ -distribution shown in Fig. 5(c2). The spectra of $^{258}\text{Md}^*$ for both energies coincide with that for SF of ^{250}Cf having the binary fission. The transfer/inelastic-induced fission should have a component that spread widely over ϕ due to momentum removed by outgoing ejectile nuclei [39]. Agreement of present spectra with that of SF indicates the absence for transfer-induced/inelastic-scattering fissions.

Absence of transfer-induced fission is also suggested by the calculation based on momentum matching condition [38, 40] to describe transfer/multinucleon-transfer process. In this model, the most probable excitation energy of a compound nucleus in transfer reaction is calculated by the reaction Q -value and number of nucleons exchanged between projectile and target nuclei. Among the $^4\text{He}+^{254}\text{Es}$ reaction, population of $^{255}\text{Es}^*$ by ejecting ^3He gives Q_{gg} value of -14.6 MeV. At the incident beam energy equal to the Coulomb barrier, the most probable excitation energy of $^{255}\text{Es}^*$ is calculated to be -14.5 MeV, thus transfer reaction cannot happen at the energies used in the experiment. For the inelastic scattering, the most probable excitation energy is $E^*=0$ MeV for $^{254}\text{Es}^*$ at the beam energy of the Coulomb barrier, again fission

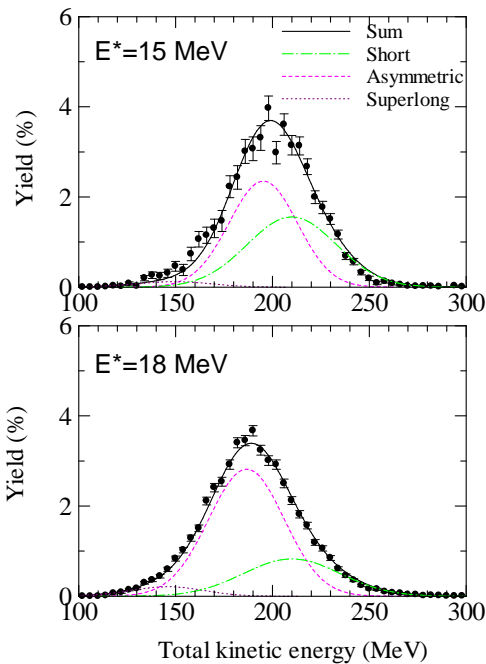


FIG. 8. (Color online) Total kinetic energy (E_k) distribution (solid circles) for $^{258}\text{Md}^*$ at $E^*=15.0$ MeV (top) and 18.0 MeV (bottom). Lines are distributions from each fission modes and their sum. Numerical expressions of the curves are shown in APPENDIX.

does not happen.

III. DISCUSSION

We decomposed the measured fission-fragment mass and TKE distributions of $^{258}\text{Md}^*$ into the AS, SH, and SL modes as explained below. The analysis is done also for $^{250}\text{Cf}(\text{SF})$ using AS and SL modes. For the procedure, we also constructed the TKE distribution for each fragment mass bin, $y(E_k|A)$, as shown in Fig. 11 ($^{250}\text{Cf}(\text{SF})$), Fig. 12, and Fig. 13 ($^{258}\text{Md}^*$) in the APPENDIX. Numerical expressions of the fitted curves are also defined in the APPENDIX. The $y(E_k|A)$ are represented by the sum of TKE distribution in each mode, $y_i(E_k|A)$ (i stands for AS, SL, or SH), which is assumed to have a Gaussian shape around the average value, $\bar{E}_{k,i}(A)$. Here, $\bar{E}_{k,i}(A)$ is defined by a quadratic shape with the maximum value in the symmetric fission.

Results of the fit to the fragment mass and TKE distributions of $^{250}\text{Cf}(\text{SF})$ are shown in Fig. 4 (b) and (c), respectively. Table I summarises the yield, average TKE, and mass-asymmetry for each fission mode. In Fig. 9, distribution of each fission mode on the mass-TKE plane are shown. Although the $^{250}\text{Cf}(\text{SF})$ is dominated by the AS mode, the SL mode is necessary to explain the drop of average TKE, $\bar{E}_k(A)$ (Fig. 4(a)) in the symmetric fission, as well as the enhanced yield in the low TKE region of $y(E_k|A)$ (Fig. 11, APPENDIX). All the parameters to

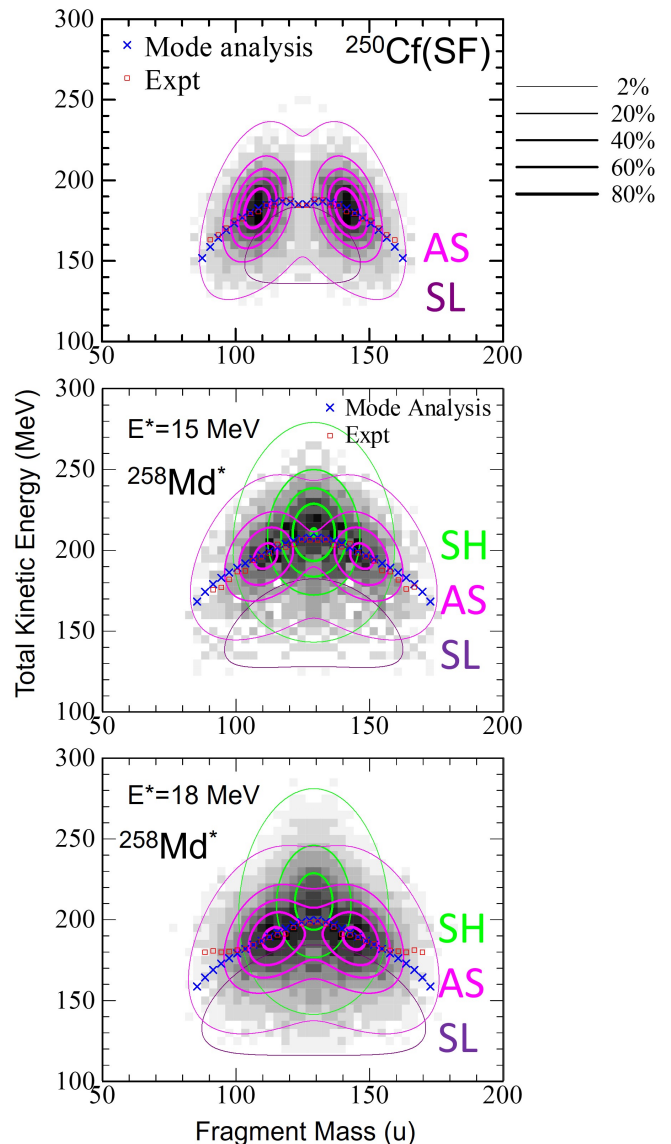


FIG. 9. (Color online) Distribution of fission mode (AS : Asymmetric, SL : Superlong, SH : Short) for $^{250}\text{Cf}(\text{SF})$ and $^{258}\text{Md}^*$ ($E^* = 15.0$ and 18.0 MeV), overlapped with experimental yield distribution, shown in Fig. 4(a) and Fig. 6. Contour lines with different thickness correspond the probability distributions to form the component with the total yield of 2, 20, 40, 60, and 80%. Cross denotes the average TKE for each fragment mass, $\bar{E}_k(A)$, obtained from the mode analysis, and is compared to the experimental data (open symbol).

describe the distribution of the fission mode are summarized in Table II of APPENDIX. To describe fission of $^{250}\text{Cf}(\text{SF})$, totally 10 parameters are necessary.

Results of the fit to the FFMD and TKE distribution of $^{258}\text{Md}^*$ are shown in Fig. 7 and Fig. 8, respectively. The fit can reasonably explain the measured FFMDs, including the flat top shape of the FFMD at $E^*=18.0$ MeV. Also, lowering of TKE by increasing the excitation energy from 15.0 to 18.0 MeV is demonstrated. In the fitting pro-

cedure, the parameters to describe distributions for each fission mode are changed between two excitation energies to better describe the measured data. For example, average TKE for AS mode changes from 195.1 MeV to 186.4 MeV (see Table I). As shown in Fig. 9, the fit well explains the location of AS mode on the mass-TKE plane. It indicates that the properties of asymmetric fission mode changes with a small excitation-energy range. The $b_{0,i}$ value for AS mode for ^{258}Md is a factor two smaller than ^{250}Cf (see TABLE II), which means that TKE of ^{258}Md decreases more moderately toward larger mass-asymmetry than ^{250}Cf . This would indicate that the AS mode behaves differently across the $A_c=257$ boundary. Alternatively, introducing another mass-asymmetric fission mode would be possible to reproduce data.

The symmetric fission mode around $\bar{E}_k=210$ MeV found in the mass-TKE plane of Fig. 6 is apparently smaller than the SS mode (233 MeV) observed in SF [11, 20, 21, 23]. Thus, we interpret it as the SH mode. The average TKE of the SH mode of $^{258}\text{Md}^*$ is about 10 MeV larger than 200 MeV for that of SF in $A_c > 257$. The difference might come from the effects of excitation energy on the potential energy surface.

Another symmetric fission mode with lower TKE than the SH mode needs to be introduced for both excitation-energy data to explain the enhanced yield of the low-TKE component of the $y(E_k|A)$ distribution at symmetric fission region, see Fig. 12 and Fig. 13 of APPENDIX. The obtained TKE for this mode are 148.8 and 145.8 MeV for $E^*=15.0$ and 18.0 MeV, respectively, which are significantly smaller than the AS mode. Considering that SL is the only mode which has lower TKE than the asymmetric fission modes in ^{250}Cf (SF) and lighter actinides of $A_c < 257$ [11], we interpret it has a feature of the SL mode.

At $E^*=15.0$ MeV, the AS and SH modes have a comparable yields of $52.0 \pm 3.5\%$ and $45.0 \pm 3.5\%$, respectively. Here, uncertainty includes statistical error and systematic error originating from the background estimation. By the increase of 3 MeV in excitation energy, the AS mode dominates with fraction $69.0 \pm 1.0\%$. All the 15 parameters to describe the distribution of fission modes for $^{258}\text{Md}^*$ are shown in Table II of APPENDIX.

We also tried to fit the ^{258}Md data by keeping the fission-mode parameters for both excitation energies and only by changing the fraction of each fission mode. For some ranges of the fragment mass and TKE, the fit curves deviate from the data points. Even in this condition, the analysis showed that the yield of asymmetric fission mode increases with excitation energy.

The mode analysis of average TKE for each fragment mass, $\bar{E}_k(A)$, for fission of $^{258}\text{Md}^*$ is shown in Fig. 9. The analysis explain the data for $E^*=15.0$ MeV. For 18.0-MeV data, the analysis underestimate the experimental data at very asymmetric region. It might imply the appearance of other mode with large mass asymmetry. But we did not additionally introduce the other mode as the statistics is not enough.

In the spontaneous fission of the region of $A_c > 257$ [20], the SH mode with $\bar{E}_k=200-205$ MeV is observed in ^{260}Md (fraction=42%), ^{259}Md (88%), ^{258}Fm (50%), ^{258}No (95%), and ^{260}Rf (100%) [20]. These studies argued that this mode is likely to extend to more heavier nuclei. In our measurement the SH mode is also identified in $^{258}\text{Md}^*$. Measured 2D spectra of mass-TKE show the appearance of asymmetric fission mode in $^{258}\text{Md}^*$, dominated in the fission of lighter region of $A_c < 257$ but not clearly identified in the heavier region of $A_c > 257$. In our fission mode analysis postulating one asymmetric and two symmetric modes, the AS and SH modes dominate and compete with each other, which would be characteristic in the region of $A_c > 257$.

We calculated fission properties of $^{258}\text{Md}^*$ by Langevin equation described by Cassinian ovals nuclear-shape parametrization. Here, the shape degree of freedom is increased from four dimensions ($\alpha, \alpha_1, \alpha_3, \alpha_4$) [41] to six dimensions ($\alpha, \alpha_1, \alpha_2, \alpha_3, \alpha_4, \alpha_5$) [42]. The calculated 2D mass-TKE spectrum is shown in Fig. 10. The results for both excitation energies can be interpreted to have dominant two fission modes, SH and AS. Furthermore, the yield of AS mode for $E^*=18.0$ MeV is larger than the 15.0 MeV spectrum. The calculation qualitatively supports present interpretation of fission-mode evolution that the yield of asymmetric fission mode increase with excitation energy. More detailed interpretation of the origin of fission modes and their competition will be discussed in detail [42]. The calculation also shows a complicated structure in the mass-TKE distribution, which would indicate the presence of different fission modes not assumed in the present analysis, due to limited statistics and difficulty to introduce larger number of fit parameters. Accumulating larger number of events would unveil the modes and their properties in more detail.

IV. CONCLUSION

We measured fission-fragment mass and TKE distributions of $^{258}\text{Md}^*$ from two excited states, $E^*=15.0$ and 18.0 MeV, populated by the $^4\text{He} + ^{254}\text{Es}$ reaction. The obtained spectra are decomposed into three fission modes; one mass-asymmetric mode and two symmetric modes with different total kinetic energy (TKE).

For the ASymmetric (AS) mode obtained in $^{258}\text{Md}^*$, the average heavy-fragment mass does not agree with the Standard 2 (ST2) reported for fission of $A_c < 257$. To make a better agreement with the measured spectrum, the TKE of AS mode need to be decreased with the amount of ≈ 9 MeV from $E^*=15.0$ to 18.0 MeV in the framework of the present fitting. Such a property would indicate the complexity of evolution of asymmetric fission mode in $A_c > 257$. The higher-TKE symmetric mode is interpreted as Short (SH) mode as its average of TKE, 210 MeV, is not so high as the Supershort (SS) mode (233 MeV) but closer to the SH mode (200 MeV), found in literature. The other symmetric-mode with small in-

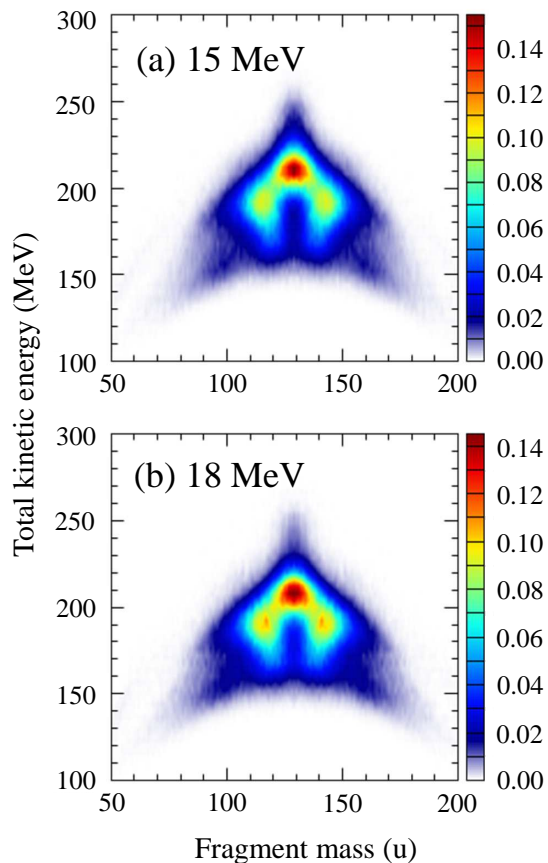


FIG. 10. (Color online) Two dimensional plot on fragment mass and TKE for fission of $^{258}\text{Md}^*$ from excitation energy of (a) $E^*=15.0$ MeV and (b) 18.0 MeV, obtained from six-dimensional Langevin calculation. The yield is normalized such that sum of the total yield becomes 200%. The color of the highest yield corresponds to the maximum value for each spectrum.

tensity has a significantly lower TKE than the AS mode, thus we interpret it has a feature of Superlong (SL).

Within the mode analysis postulated in this work, the AS and SH modes have a comparative yield at the excitation energy of $E^*=15.0$ MeV. By increasing the energy to $E^*=18.0$ MeV, enhancement of AS mode is indicated. Change of the yield between fission modes in such a small excitation energy interval indicates a strong competition between different fission modes in $A_c > 257$.

We attempted the 6-dimensional Langevin calculation to describe fission of $^{258}\text{Md}^*$. The obtained mass-TKE distribution indicates the increasing yield of AS fission mode from 15.0 MeV to 18.0 MeV, supporting the mode analysis given above.

It is interesting to take fission data for a wider range of nuclei beyond the $A_c=257$ boundary. Such experiment is possible using the setup of multinucleon-transfer induced fission [43, 44], developed and applied at JAEA.

ACKNOWLEDGMENTS

We thank the crew of the JAEA tandem accelerator facility for supplying a high-quality stable beam. Special thanks for calculating FFMDs are due to Dr. P. Möller and Prof. I. Tsekhanovich. AA was partially supported by the STFC UK grant. This research was also supported by the Office of Nuclear Physics, U.S. Department of Energy (U.S. DOE) under contract DE-AC05-00OR22725 and by the U.S. DOE Isotope Program. The six-dimensional Langevin calculation was performed with the JAEA supercomputer HPE SGI8600.

V. APPENDICES

We define the normalized distribution of total kinetic energy of fragments (E_k) for each fission mode (AS : ASymmetric, SH : SHort, SL : SuperLong) in each fission-fragment with mass A as

$$\sum_{E_k} w_{\text{AS}}(E_k|A)\Delta E_k = 1, \quad (1)$$

$$\sum_{E_k} w_{\text{SL}}(E_k|A)\Delta E_k = 1, \quad (2)$$

$$\sum_{E_k} w_{\text{SH}}(E_k|A)\Delta E_k = 1. \quad (3)$$

ΔE_k is the E_k -bin width adopted in the analysis. We do not discuss Supershort (SS) mode as it was no evident in our measurement of $^{258}\text{Md}^*$. For the asymmetric fission mode, we include only one mode, having a feature of Standard 2 [11]. By replacing the subscript to represent fission mode to "i", the above expressions can be represented as

$$\sum_{E_k} w_i(E_k|A)\Delta E_k = 1. \quad (4)$$

For each mode "i", the average TKE values for fragment A is represented as

$$\bar{E}_{k,i}(A) = \frac{\sum_{E_k} E_k w_i(E_k|A)\Delta E_k}{\sum_{E_k} w_i(E_k|A)\Delta E_k}. \quad (5)$$

In the analysis, the average TKE in Eq.(5) is represented by the following expression using fitting parameters of $a_{0,i}$ and $b_{0,i}$, for each mode "i",

$$\bar{E}_{k,i}(A) = a_{0,i} - b_{0,i}(A - A_c/2)^2, \quad (6)$$

where A_c is the mass of fissioning nucleus.

TKE distribution for each fragment A is represented by the weighted sum of w_i over fission modes

$$y(E_k|A) = \sum_i p_i(A)w_i(E_k|A). \quad (7)$$

Here, $p_i(A)$ is the fraction of each fission mode "i" to form the yield of fission-fragment A , $Y(A)$, as

$$Y(A) = \sum_i p_i(A). \quad (8)$$

$p_i(A)$ is represented by

$$p_i(A) = \frac{f_i}{\sqrt{2\pi}\sigma_{A,i}} \exp\left\{-\frac{(A - \bar{A}_{H,i})^2}{2\sigma_{A,i}^2}\right\} + \frac{f_i}{\sqrt{2\pi}\sigma_{A,i}} \exp\left\{-\frac{(A - (A_c - \bar{A}_{H,i}))^2}{2\sigma_{A,i}^2}\right\}, \quad (9)$$

where f_i , $\bar{A}_{H,i}$ and $\sigma_{A,i}$ are the fraction of the mode "i", average-heavy fragment mass, and standard deviation, respectively, and are determined in the fitting procedure. Here,

$$\sum_i f_i = 100 \text{ (\%)} \quad (10)$$

holds. Distribution of $Y(A)$ and $p_i(A)$ are shown in Fig. 4(b) and Fig. 7(upper panel), for $^{250}\text{Cf}(\text{SF})$ and $^{258}\text{Md}^*$, respectively.

Then, $w_i(E_k|A)$ is represented by

$$w_i(E_k|A) = \frac{1}{\sqrt{2\pi}\sigma_{E_k,i}} \exp\left\{-\frac{(E_k - \bar{E}_{k,i}(A))^2}{2\sigma_{E_k,i}^2}\right\}. \quad (11)$$

Here, $\bar{E}_{k,i}(A)$ is defined by Eq.(6). We assume that the standard deviation $\sigma_{E_k,i}$, determined by the fitting procedure, for a specific fission mode "i" is kept constant over all the fragment mass (A) range.

For comparison of the measured TKE-distribution in each fragment A , we define the normalized distribution of Eq.(7) using

$$\hat{y}(E_k|A) = \frac{\sum_i p_i(A)w_i(E_k|A)}{\sum_{E_k} \sum_i p_i(A)w_i(E_k|A)\Delta E_k}. \quad (12)$$

The distributions of Eq.(12) for $^{250}\text{Cf}(\text{SF})$, $^{258}\text{Md}^*$ ($E^*=15$ MeV), and $^{258}\text{Md}^*$ ($E^*=18$ MeV), obtained after

fitting, are shown in Fig. 11, Fig. 12, and Fig. 13, respectively, in comparison with experimental data.

Average kinetic energy of fragment mass A is calculated by

$$\bar{E}_k(A) = \frac{\sum_{E_k} E_k y(E_k|A) \Delta E_k}{\sum_{E_k} y(E_k|A) \Delta E_k}. \quad (13)$$

The curves for $^{250}\text{Cf}(\text{SF})$ and $^{258}\text{Md}^*$ ($E^*=15.0$ and 18.0 MeV) are shown in Fig. 4(a) and Fig. 9, respectively.

Projection of mass-TKE distribution on the TKE axis is represented by

$$Y(E_k) = \frac{1}{2} \sum_A y(E_k|A) \Delta A, \quad (14)$$

where the factor $\frac{1}{2}$ is applied to give

$$\sum_{E_k} Y(E_k) \Delta E_k = 100 \text{ (\%)}. \quad (15)$$

The TKE distribution for each mode "i" is defined by

$$Y_i(E_k) = \frac{1}{2} \sum_A p_i(A) w_i(E_k|A) \Delta A. \quad (16)$$

$Y(E_k)$ and $Y_i(E_k)$ are shown in Fig. 4(c) and Fig. 8 for $^{250}\text{Cf}(\text{SF})$ and $^{258}\text{Md}^*$, respectively.

Finally FFMDs constructed using the TKE values lower and higher than 200 MeV can be represented by

$$Y_{>200\text{MeV}}(A) = \sum_{E_k > 200\text{MeV}} y(E_k|A) \Delta E_k, \quad (17)$$

$$Y_{\leq 200\text{MeV}}(A) = \sum_{E_k \leq 200\text{MeV}} y(E_k|A) \Delta E_k. \quad (18)$$

The curves are shown in Fig. 7 in the main text.

Parameters obtained in the analysis are summarized in Table II. To describe fission of $^{250}\text{Cf}(\text{SF})$, totally 10 parameters are necessary to include two fission modes (AS and SL). For the fission of $^{258}\text{Md}^*$, 15 parameters needs to be determined to include three fission modes.

[1] O. Hahn and F. Straßmann, *Naturwissenschaften* **27**, 11 (1939).
 [2] L. Meitner and O.R. Frisch, *Nature (London)* **143**, 239 (1939).
 [3] N. Bohr and J.A. Wheeler, *Phys. Rev.* **56**, 426 (1939).
 [4] V.M. Strutinsky, *Nucl. Phys.* **A95**, 420 (1967).
 [5] V.M. Strutinsky, *Nucl. Phys.* **A122**, 1 (1968).
 [6] M. Brack, J. Damgaard, A.S. Jensen, H.C. Pauli, V.M. Strutinsky, C.Y. Wong, *Rev. Mod. Phys.* **44**, 320 (1972).

[7] S. Bjørnholm and J.E. Lynn, *Rev. Mod. Phys.* **52**, 725 (1980).
 [8] P. Möller and J.R. Nix, *Proceedings of a Symposium on Physics and Chemistry of fission*, Rochester, New York, 13-17 August 1973, Vol. I, P.103.
 [9] P. Möller, D.G. Madland, A.J. Sierk, A. Iwamoto, *Nature* **409**, 785 (2001).
 [10] A.N. Andreyev, K. Nishio, K.H. Schmidt, *Rep. Prog. Phys.* **81**, 016301 (2018).
 [11] U. Brosa, S. Großmann, and A. Müller, *Phys. Rep.* **197**,

TABLE II. Parameters to describe fission mode, Asymmetric (AS), Short (SH), and Superlong (SL), for $^{250}\text{Cf}(\text{SF})$ and $^{258}\text{Md}^*$ ($E^*=15.0, 18.0\text{ MeV}$). Center of fragment mass for symmetric fission mode is shown in square brackets.

$^{250}\text{Cf}(\text{SF})$							
Mode,i	f_i (%)	$\bar{A}_{H,i}$ (u)	$\sigma_{A,i}$ (u)	$a_{0,i}$ (MeV)	$b_{0,i}$ (MeV/u ²)	$\sigma_{Ek,i}$ (MeV)	
AS	97.0±2.0	142.0±0.5	7.1±0.2	190±2	0.025±0.002	17.0±0.5	
SH	-	-	-	-	-	-	
SL	3.0±2.0	[125.0]	18.0±5.0	160±5	0.025±0.010	20.0±5.0	
$^{258}\text{Md}(E^*=15.0\text{ MeV})$							
Mode,i	f_i (%)	$\bar{A}_{H,i}$ (u)	$\sigma_{A,i}$ (u)	$a_{0,i}$ (MeV)	$b_{0,i}$ (MeV/u ²)	$\sigma_{Ek,i}$ (MeV)	
AS	52.0±3.5	147.0±1.0	9.7±0.3	200.5±1.0	0.013±0.003	17.0±1.0	
SH	45.0±3.5	[129.0]	10.2±0.5	211.0±1.0	0.010±0.005	23.0±0.5	
SL	3.0±1.0	[129.0]	22.0±10.0	155.0±5.0	0.015±0.010	18.0±5.0	
$^{258}\text{Md}(E^*=18.0\text{ MeV})$							
Mode,i	f_i (%)	$\bar{A}_{H,i}$ (u)	$\sigma_{A,i}$ (u)	$a_{0,i}$ (MeV)	$b_{0,i}$ (MeV/u ²)	$\sigma_{Ek,i}$ (MeV)	
AS	69.0±1.0	144.5±0.5	10.5±0.5	191.0±1.0	0.013±0.003	19.0±1.0	
SH	26.0±1.0	[129.0]	10.0±0.5	211.0±2.0	0.010±0.005	25.0±3.0	
SL	5.0±2.0	[129.0]	22.0±3.0	150.0±5.0	0.010±0.005	18.0±5.0	

- 167 (1990).
- [12] C. Wagemans, *The Nuclear Fission Process*, CRC Press (1991).
- [13] D.C. Hoffman and M.R. Lane, *Radiochimica Acta* 70/71, 135 (1995).
- [14] K.-H. Schmidt, S. Steinhäuser, C. Böckstiegel, A. Grewe, A. Heinz, A.R. Jungmans, J. Benlliure, H.-G. Clerc, M. de Jong, J. Müller, M. Pfützner, B. Voss, *Nucl. Phys. A* **665**, (2000) 221.
- [15] C. Böckstiegel, S. Steinhäuser, K.-H. Schmidt, H.-G. Clerc, A. Grewe, A. Heinz, M. de Jong, A.R. Jungmans, J. Müller, B. Voss, *Nucl. Phys. A* **802**, 12 (2008).
- [16] J.-F. Martin, J. Taïeb, G. Boutoux, A. Chatillon, T. Gorbine, E. Pellereau, L. Audouin, A. Heinz, H. Alvarez-Pol, Y. Ayyad, G. Bélier, J. Benlliure, M. Caamaño, E. Casarejos, D. Cortina-Gil, A. Ebran, F. Farget, B. Fernández-Domínguez, L. Grente, H.T. Johansson, B. Jurado, A. Kelić-Heil, N. Kurz, B. Laurent, C. Nociforo, C. Paradela, S. Pietri, A. Prochazka, J.L. Rodríguez-Sánchez, D. Rossi, H. Simon, L. Tassan-Got, J. Vargas, B. Voss, H. Weick, *Phys. Rev. C* **104**, 044602 (2021).
- [17] A. Chatillon, J. Taïeb, H. Alvarez-Pol, L. Audouin, Y. Ayyad, G. Bélier, J. Benlliure, G. Boutoux, M. Caamaño, E. Casarejos, D. Cortina-Gil, A. Ebran, F. Farget, B. Fernández-Domínguez, T. Gorbine, L. Grente, A. Heinz, H.T. Johansson, B. Jurado, A. Kelić-Heil, N. Kurz, B. Laurent, J.-F. Martin, C. Nociforo, C. Paradela, E. Pellereau, S. Pietri, A. Prochazka, J.L. Rodríguez-Sánchez, D. Rossi, H. Simon, L. Tassan-Got, J. Vargas, B. Voss, H. Weick, *Phys. Rev. Lett.* **124**, 202502 (2020).
- [18] G. Scamps and C. Simenel, *Nature* **564**, 382 (2018).
- [19] E.K. Hulet, J.F. Wild, R.J. Dougan, R.W. Loughheed, J.H. Landrum, A.D. Dougan, M. Schädel, R.L. Hahn, P.A. Baisden, C.M. Henderson, R.J. Dupzyk, K. Sümmerner, G.R. Bethune, *Phys. Rev. Lett.* **56**, 313 (1986).
- [20] E.K. Hulet, J.F. Wild, R.J. Dougan, R.W. Loughheed, J.H. Landrum, A.D. Dougan, P.A. Baisden, C.M. Henderson, R.J. Dupzyk, R.L. Hahn, M. Schädel, K. Sümmerner, G.R. Bethune, *Phys. Rev. C* **40**, 770 (1989).
- [21] R.W. Loughheed, E.K. Hulet, J.F. Wild, K.J. Moody, R.J. Dougan, C.M. Gannett, R.A. Henderson, D.C. Hoffman, and D.M. Lee, *Proceedings of 50 years with nuclear fission*, p.694 Volume 2 (1989).
- [22] J.F. Wild, E.K. Hulet, R.W. Loughheed, K.J. Moody, B.B. Bandong, R.J. Dougan, and A. Veck, *J. Alloys and Compounds*, **213/214**, 86 (1994).
- [23] J.F. Wild, J. van Aarle, W. Westmeier, R.W. Loughheed, E.K. Hulet, K.J. Moody, R.J. Dougan, E.-A. Koop, R.E. Glaser, R. Brandt, P. Patzelt, *Phys. Rev. C* **41**, 640 (1990).
- [24] D.C. Hoffman, J.B. Wilhelmy, J. Weber, W.R. Daniels, E.K. Hulet, R.W. Loughheed, J.H. Landrum, J.F. Wild, R.J. Dupzyk, *Phys. Rev. C* **21** 972 (1980).
- [25] W. John, E.E. Hulet, R.W. Loughheed, J.J. Wesolowski, *Phys. Rev. Lett.* **27** 45 (1971).
- [26] A. Pal, S. Santra, P.C. Rout, R. Gandhi, A. Baishya, T. Santhosh, R. Tripathi, T.N. Nag, *Phys. Rev. C* **104**, L031602 (2021).
- [27] I.M. Itkis, M.G. Itkis, G.N. Knyazheva, E.M. Kozulin, T.A. Loktev, K.V. Novikov, F. Hanappe, and E. Vardaci, *J. Phys. Conf. Ser.* **515**, 012008 (2014).
- [28] H.C. Britt, D.C. Hoffman, J. van der Plicht, J.B. Wilhelmy, E. Cheifetz, R.J. Dupzyk, and R.W. Loughheed, *Phys. Rev. C* **30**, 559 (1984).
- [29] S. Tanaka, Y. Aritomo, Y. Miyamoto, K. Hirose, and K. Nishio, *Phys. Rev. C* **100**, 064605 (2019).
- [30] <https://www.nndc.bnl.gov/nudat3/>
- [31] <https://neutrons.ornl.gov/hfir>
- [32] I. Tsekhanovich, A.N. Andreyev, K. Nishio, D. Denis-Petit, K. Hirose, H. Makii, Z. Matheson, K. Morimoto, K. Morita, W. Nazarewicz, R. Orlandi, J. Sadhukhanh, T. Tanaka, M. Vermeulen, M. Warda, *Phys. Lett. B* **790**, 583 (2019).
- [33] D.C. Hoffman, G.P. Ford, J.P. Balagna, *Phys. Rev. C* **7**, 276 (1973).
- [34] V.E. Viola, K. Kwiatkowski, and M. Walker, *Phys. Rev. C* **31**, 1550 (1985).
- [35] H. Thierens, A. De Clercq, E. Jacobs, D. De Frenne, P. D'hondt, P. De Gelder, A.J. Deruytter, *Phys. Rev. C*,

- 23**, 2104 (1981).
- [36] K.-H. Schmidt, B. Jurado, C. Amouroux, and C. Schmitt, Nuclear Data Sheets **131**, 107 (2016).
- [37] Average spin was calculated with the code based on the CCFULL, K. Hagino, N. Rowley, A.T. Kruppa, Comput.Phys. Commun.**123**, 143 (1999).
- [38] M.J. Vermeulen, K. Nishio, K. Hirose, K.R. Kean, H. Makii, R. Orlandi, K. Tsukada, I. Tsekhanovich, A.N. Andreyev, S. Ishizaki, M. Okubayashi, S. Tanaka, and Y. Aritomo, Phys. Rev. C **102**, 054610 (2020).
- [39] K. Nishio, H. Ikezoe, S. Mitsuoka, I. Nishinaka, Y. Nagame, Y. Watanabe, T. Ohtsuki, K. Hirose, and S. Hofmann, Phys. Rev. C **77**, 064607 (2008).
- [40] Y. Alhassid, R.D. Levine, J.S. Karp, and S.G. Steadman, Phys. Rev. C **20**, 1789 (1979).
- [41] K. Okada, T. Wada, R. Capote, N. Carjan, Phys. Rev. C **107**, 034608 (2023).
- [42] K. Okada, K. Nishio, T. Wada, N. Carjan, to be published.
- [43] R. Léguillon, K. Nishio, K. Hirose, H. Makii, I. Nishinaka, R. Orlandi, K. Tsukada, J. Smallcombe, S. Chiba, Y. Aritomo, T. Ohtsuki, R. Tatsuzawa, N. Takaki, N. Tamura, S. Goto, I. Tsekhanovich, C.M. Petrachei, A.N. Andreyev, Phys. Lett. B **761**, 125 (2016).
- [44] K. Hirose, K. Nishio, S. Tanaka, R. Léguillon, H. Makii, I. Nishinaka, R. Orlandi, K. Tsukada, J. Smallcombe, M.J. Vermeulen, S. Chiba, Y. Aritomo, T. Ohtsuki, K. Nakano, S. Araki, Y. Watanabe, R. Tatsuzawa, N. Takaki, N. Tamura, S. Goto, I. Tsekhanovich, and A.N. Andreyev, Phys. Rev. Lett. **119**, 222501 (2017).

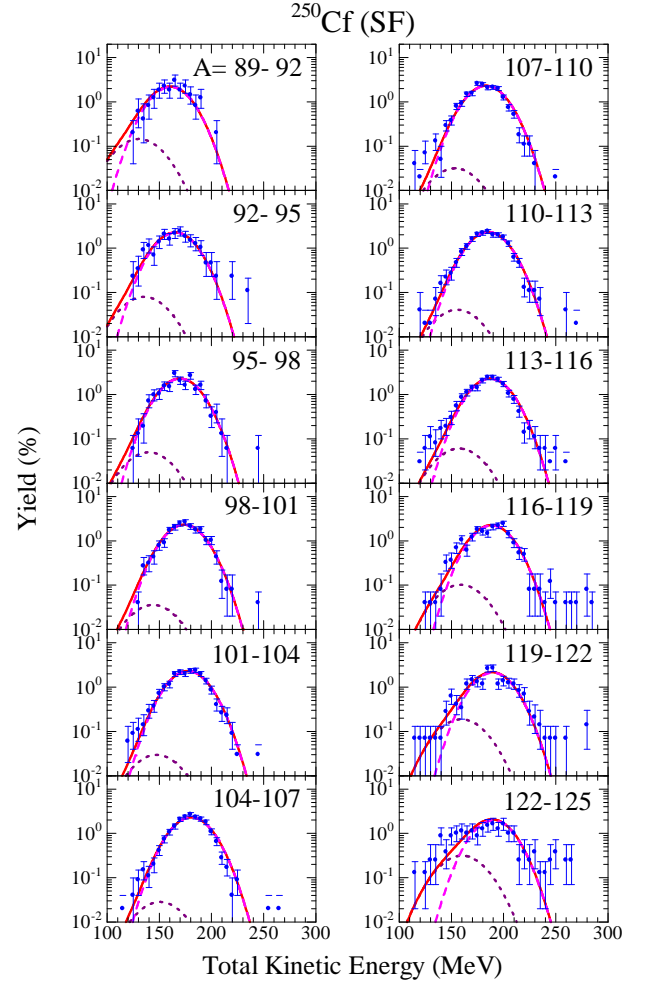


FIG. 11. (Color online) Total kinetic energy (TKE) distribution for each bin of fragment mass A , $\hat{y}(E_k|A)$, obtained in spontaneous fission of ^{250}Cf (solid circles). The spectrum is normalized such that the sum of the yield over TKE becomes 100%. Contribution from Asymmetric (dashed curve) and Superlong mode (dotted curve) obtained in the analysis are shown as well as their sum (solid curve).

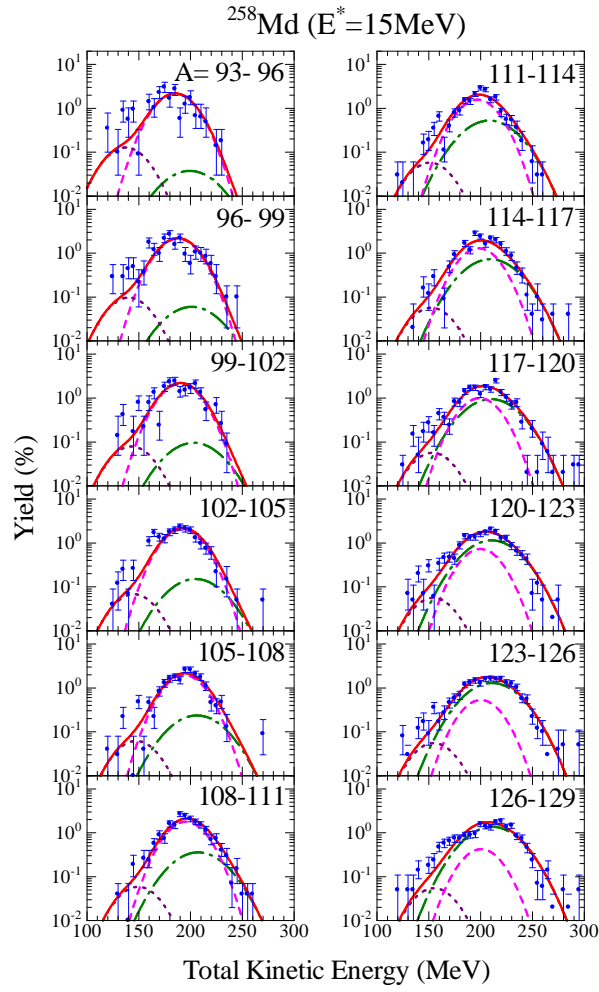


FIG. 12. (Color online) Same as FIG.11, but for fission of $^{258}\text{Md}^*$ obtained at $E^* = 15.0\text{MeV}$ (solid circles). Yields for Asymmetric (dashed curve), Short (dash-dotted curve), and Superlong mode (dotted curve) are shown as well as their sum (solid curve).

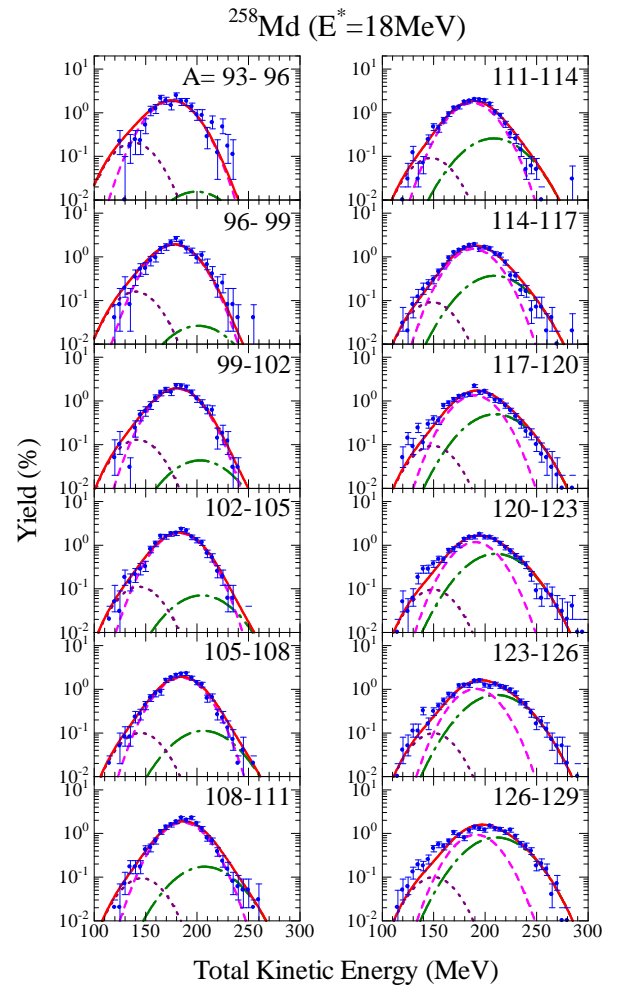


FIG. 13. (Color online) Same as FIG.11, but for fission of $^{258}\text{Md}^*$ obtained at $E^* = 18.0\text{MeV}$ (solid circles). Yields for Asymmetric (dashed curve), Short (dash-dotted curve), and Superlong mode (dotted curve) are shown as well as their sum (solid curve).